International Journal of Microwave and Wireless Technologies, 2017, 9(7), 1447–1452.
doi:10.1017/S1759078716001434

RESEARCH PAPER

Study of dual-band inline mixed coupled BPF design and two transmission zero pairs controlling mechanism

DI LU[1,2], TENG-FEI YAN[1] AND XIAO-HONG TANG[1]

In this letter, a passive high-selectivity dual-band filter with two controllable transmission zero (TZ) pairs is proposed, while synthesis method and control mechanism of the two TZ pairs are investigated. Specifically, by employing the magnetic/electric mixed coupling (MEMC), source–load coupling (S–L coupling) and stepped-impedance resonators, a dual-band bandpass filter with two pairs of controllable TZs is constructed. Two controllable TZ pairs can be independently adjusted by re-modifying the associated coupling structures. To validate the synthesizability and controllability of the TZ pairs, mathematical synthesis, and EM simulations are carried out. Two demonstrative filters with identical passband performance and different central TZ distributions for GSM (0.9/1.8 GHz) are designed and measured. The analysis and experimental results show that the synthesis-controllable TZ pair (f_{z2}, f_{z3}) introduced by MEMC can be synthesized and controlled using inline mixed coupling synthesis, and the optimization-controllable TZ pair (f_{z1}, f_{z4}) because of S–L coupling is controlled by S–L coupling strength optimization procedure.

Keywords: TZ pair synthesis, Controllable TZ pairs, MEMC, S–L coupling, Stepped-impedance resonator, Dual-band BPF

Received 22 July 2016; Revised 5 December 2016; Accepted 7 December 2016; first published online 10 January 2017

I. INTRODUCTION

The increasingly congestible frequency spectrum has raised the new requirements for the dual-band service and the dual-band communication system. Targeted interference suppression and high-yield stopband rejection using finite transmission zeros (TZs) to meet the requirements is becoming one of the challenges for dual-band filter design. The controllable TZ, which is directly derived from general Chebyshev functions or other prototype filtering functions and can be placed using the filter function synthesis techniques, is defined as the synthesis-controllable TZ. Thus far, two types of basic synthesis methods, cross coupling [1] and source/load coupling (S–L coupling) [2], were used to introduce the synthesis-controllable TZ pair from the fully canonical single-band bandpass filters (BPFs) for the dual-band BPFs. However, it is not very suitable to implement large-separation passbands. On the other hand, when a TZ does not appear in the initial prototype filtering functions but can be excited and adjusted by using optimization procedures without significantly affecting the passband response, such TZ is defined as the optimization-controllable TZ. For dual-band filter, separately using S–L coupling or magnetic/electric mixed coupling (MEMC) (did not be synthesized) to introduce and control this type of TZs have been reported recently. By changing S–L coupling strength, all TZs are jointly adjusted as described in [3, 4], and, by controlling the magnetic coupling (M-coupling) and the electric coupling (E-coupling) structures, a single pair of TZ is adjusted, as described in [5]. Whereas, compared to the synthesis techniques [1, 2], the challenge of the optimization-controllable TZ research [3–5] has still laid on how to control all of the TZs and enhance the TZ controllability (independent control) in the dual-band BPF design.

In addition, many high-performance dual-band BPF have been reported in recently years. In [6], a compact size and low insertion loss dual-band BPF based on spiral-line loops resonator was presented. However, TZs, center frequency, and bandwidth were not controllable, and TZs operation mechanism was not included. In [7], a dual-band filter with total five TZs using multimode resonators was proposed, but the TZs could not be independently controllable. In [8, 9] using short-circuit centered stepped impedance resonators with MEMC or 0° feeding lines with lowpass filtering structure to realize multiple TZs and a wide stopband in the dual-band BPF were demonstrated, but the compromised insertion loss and TZ control were not discussed.

In this paper, jointly using MEMC and S–L coupling in a dual-band BPF to approach two controllable TZ pairs is studied. By employing the inline mixed coupling synthesis [10], a synthesis-controllable TZ pair due to MEMC is rigorously

[1]School of Electronic Engineering, University of Electronic Science and Technology of China (UESTC), Qingshuihe Campus: No.2006, Xiyuan Ave, West Hi-Tech Zone, Chengdu, Sichuan, China
[2]Charles L. Brown Department of Electrical and Computer Engineering, University of Virginia, 351 McCormick Road, Charlottesville, VA, USA
Corresponding author:
D. Lu
Email: ludi888abc@hotmail.com, 201311020205@std.uestc.edu.cn

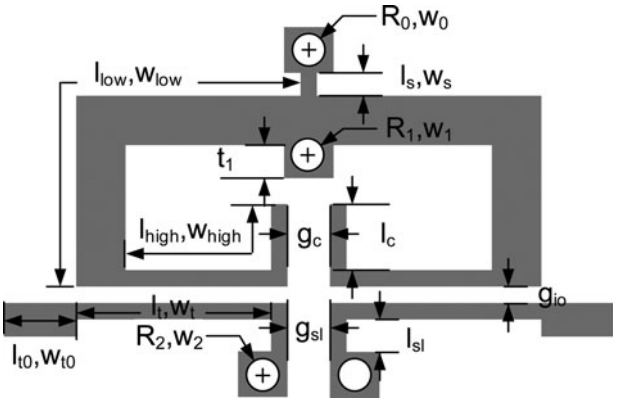

Fig. 1. Geometric structure of the proposed filter (the vias with radius of R_o, R_1, and R_2 are shorted to ground).

synthesized, which can be placed as desired by choosing the appropriate E/M-coupling ratio or

$$\begin{bmatrix} 0 & k_{S1x} & 0 & k_{SLx} \\ k_{S1x} & 0 & k_{12x} & 0 \\ 0 & k_{12x} & 0 & k_{2Lx} \\ k_{SLx} & 0 & k_{2Lx} & 0 \end{bmatrix}, \quad Q_{ex} = \frac{FBW}{k_{01x}^2},$$

J/K-inverter ratio. The other controllable TZ pair, which can be adjusted by adjusting the S–L coupling strength, is verified by EM simulation. In addition, the center frequencies of the proposed filter are specified by properly selecting the high–low impedance ratio and the electric length ratio of stepped-impedance resonators (SIRs), as discussed in [11]. For validation, two filters operating at 0.9/1.8 GHz (GSM band) with different central TZ pair (synthesis-controllable TZ pair) distribution are implemented and measured. The experimental results validate the analysis and also exhibit the TZ shifting feature.

II. EQUIVALENT CIRCUIT AND TZS ANALYSIS

As shown in Fig. 1, the proposed filter consists of two coupled $\lambda/4$ SIRs with a high/low-impedance section and two shorted feeding lines. Two common grounding vias R_o and R_1, and a high-impedance line l_s behave as an M-coupling inductance L_s as well as a part of K-inverter. The high-impedance parallel coupling lines with a length of l_c and adjacent spacing of g_c are treated as a parallel-resonant tank as well as a part of J-inverter. Additionally, the shorted feeding lines with a length of l_{sl} and adjacent spacing of g_{sl} construct the S–L coupling. The coupling diagram is shown in Fig. 2(a).

The coupling mechanism between two SIRs is illustrated in Figs 2(b) and 2(c). Under the resonant condition [11] and the pressed values, $\theta_l = \theta_h = \theta_o$, $Z_h = R_z Z_l = R_z Z_o$, the coupling coefficient k and Y_{21} in the admittance matrix can be expressed as

$$k = \frac{\omega_o^2 - \omega_e^2}{\omega_o^2 + \omega_e^2} \approx M_{12} - E_{12} = \frac{K_s}{x} - \frac{J_g}{b} \to J_g = \left(\frac{K_s}{x - k}\right) b, \tag{1}$$

$$Y_{21} = \frac{jJ_g}{R_t^2 J_g^2 Z_o^2 \sin^2\theta_o - \cos^2\theta_o} + \frac{jK_s}{Z_o^2 \sin^2\theta_o - K_s \cos^2\theta_o}, \tag{2}$$

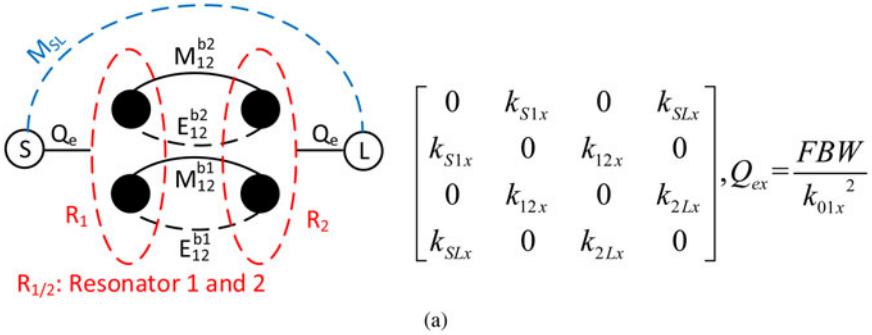

$$\begin{bmatrix} 0 & k_{S1x} & 0 & k_{SLx} \\ k_{S1x} & 0 & k_{12x} & 0 \\ 0 & k_{12x} & 0 & k_{2Lx} \\ k_{SLx} & 0 & k_{2Lx} & 0 \end{bmatrix}, Q_{ex} = \frac{FBW}{k_{01x}^2}$$

(a)

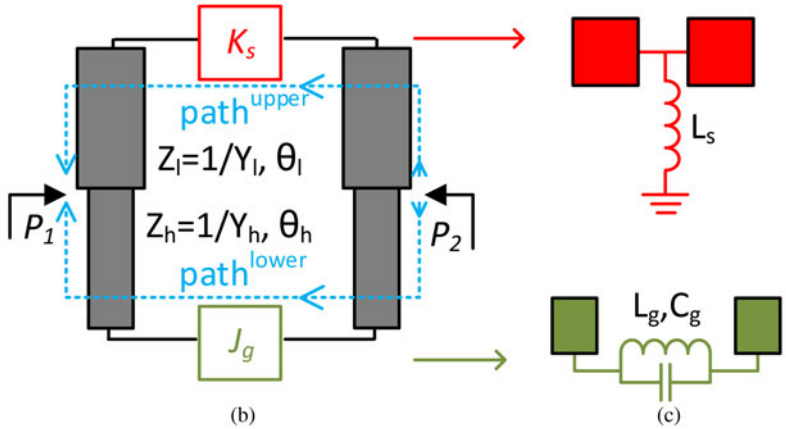

Fig. 2. (a) Coupling diagram (M: M-coupling; E: E-coupling; b1/b2: band 1 or 2). (b) Equivalent circuit of two mixed coupling SIRs. (c) Equivalent circuit of J and K inverters.

https://doi.org/10.1017/S1759078716001434 Published online by Cambridge University Press

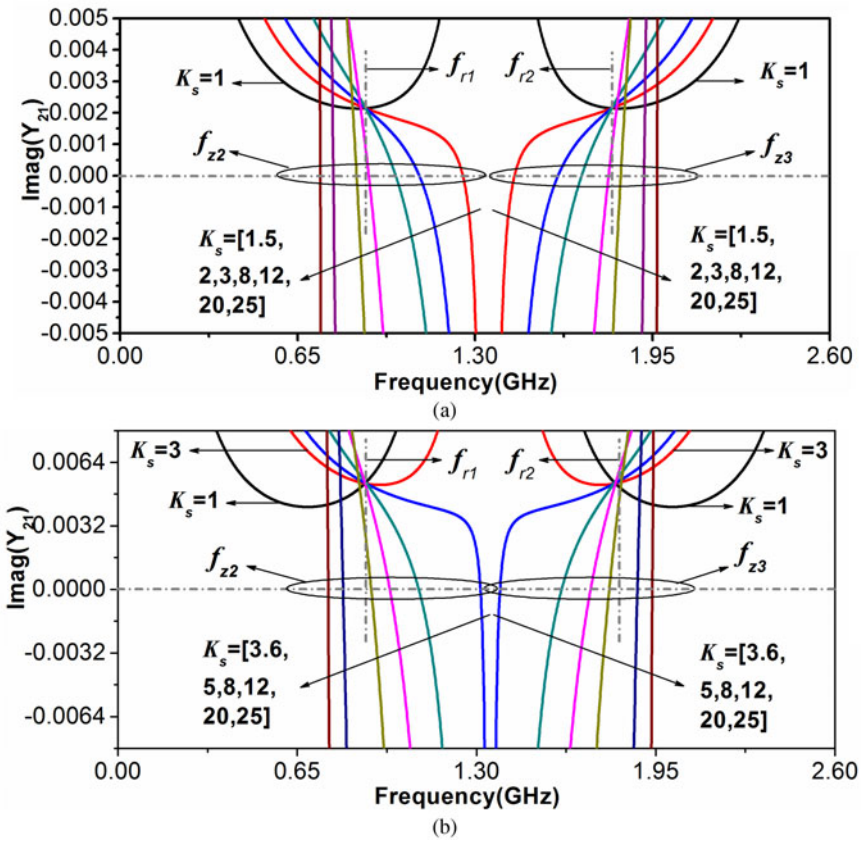

Fig. 3. Admittance graphs versus different K_s with constant coupling coefficient k (when imag (Y_{21}) is equal to zero, the TZ pair emerges) (a) $f_o = 0.9$ GHz, $k = 0.046$, $b = 0.0116$, and $x = 31.4159$ for band 1. (b) $f_o = 1.8$ GHz, $k = 0.057$, $b = 0.0233$, and $x = 62.8319$ for band 2. (Three key cases, $K_s = 1.5$, 2, 12 for (a) or $K_s = 3.6$, 5, 20 for (b), are noted. The first case is when the pair of TZ splits apart; the second case is when the TZ pair move toward the passbands, and the last case is when the TZ pair has moved through the passbands.)

$$b = \frac{\omega_o}{2}\frac{dB}{d\omega}\bigg|_{\omega=\omega_o}, \quad B = Y_h\frac{-Y_l + Y_h\tan^2\theta_o}{(Y_h + Y_l)\tan\theta_o} = Y_h\frac{\tan^2\theta_o - Rt}{(1 + Rt_l)\tan\theta_o}, \tag{3}$$

$$x = \frac{\omega_o}{2}\frac{dX}{d\omega}\bigg|_{\omega=\omega_o}, \quad X = Z_l\frac{-Z_h + Z_l\tan^2\theta_o}{(Z_l + Z_h)\tan\theta_o} = \frac{Z_h}{Rt}\frac{\tan^2\theta - Rt}{(1 + Rt)\tan\theta}, \tag{4}$$

where ω_o and ω_e respectively denote the odd- and even-mode resonant angular frequency. E-coupling E_{12} and M-coupling M_{12} are expressed by J_g/b, and K_s/x. Herein, b and x are derived from (3) and (4). B and X indicate the input susceptance and reactance, respectively. M-coupling is dominant when $K_s/x > J_g/b$ and E-coupling is dominant when $K_s/x < J_g/b$.

By substituting (1) into (2), the relationship between Y_{21} and K_s with a constant total coupling coefficient k can be obtained. In other words, we can choose a different pair of J_g and K_s resulting in different Y_{21} while keeping the passbands unchanged. Figure 3 depicts the graphs of the admittance for center frequency $f_o = 0.9$ GHz (band 1), $k = 0.046$, and $f_o = 1.8$ GHz (band 2), $k = 0.057$ with K_s ranged from 1 to 25 when $R_z = 3$, $\theta_o = \pi/3$ and $Z_o = 30\,\Omega$ are set. It can be found a pair of TZs (imag(Y_{21}) = 0) emerge when $K_s = 1.5$ for band 1 and $K_s = 3.6$ for band 2, and then split afterward. Furthermore, when $K_s > 8$ for band 1 or $K_s > 12$ for band 2 is defined, $f_{z2} < f_{r1}$ and $f_{z3} > f_{r2}$ can be observed (f_{r1} and f_{r2} are self-resonant frequencies), which means, that f_{z2} shifts to the lower side of the first band and f_{z3} shifts to the upper side of the second band, respectively. Hence, the central pair of TZs (f_{z2}, f_{z3}) are simultaneously synthesized. Noted herein, since the coupling coefficients are frequency dependent in this graph, the fact that f_{z2} and f_{z3} are respectively synthesized using the first-band coefficient and the second-band coefficient, are used for the more precise TZ pair synthesis.

For the quantitative analysis, Rogers RO5880 substrate ($\varepsilon_r = 2.2$) with a thickness of 0.508 mm is utilized as the dielectric and commercial software ANSYS HFSS is employed for calculation. Figure 4 plots the extracted design Q_e graph for two bands.

In order to get the smaller inductive K-inverter, two larger vias are employed instead of the small one, as shown in Fig. 5(a). In addition, the capacitive J-inverter is realized with the parallel coupled line, as given in Fig. 5(b)

The impacts to two band couplings, which are induced by M-coupling perturbation and exerting on the total coupling coefficients k, are depicted in Fig. 6(a). When k changes from the negative value (E-coupling) to the positive one (M-coupling), the TZ (f_{z2} or f_{z3}) and the odd mode (for two bands) shift from one side of the passband to the other. Figure 6(b) plots extracted K and J from different coupling structures with different physical dimensions.

https://doi.org/10.1017/S1759078716001434 Published online by Cambridge University Press

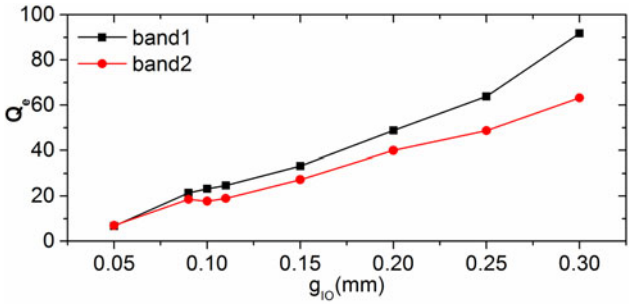

Fig. 4. Simulated external quality factor by changing g_{io}, when $l_t = 27.42$ mm and $w_t = 0.2$ mm.

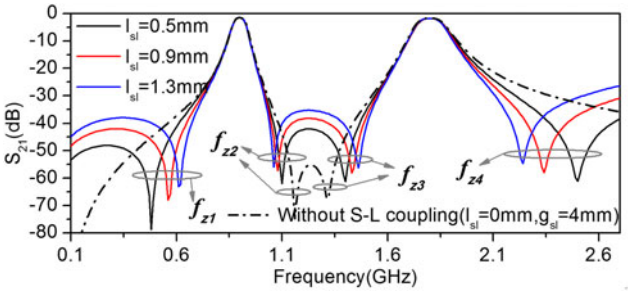

Fig. 7. Simulated S_{21} (dB) against the different S–L coupling strength.

On the other hand, adding S–L coupling introduces two optimization-controllable TZs (f_{z1}, f_{z4}) which are simultaneously controlled by the coupling strength (l_{ls} and g_{ls}) with a small impact on the other pair of TZs, as shown in Fig. 7. It is noted that when f_{z2} is higher than f_{z4}, or f_{z3} is lower than f_{z1}, the associated TZ pair will disappear. As a result, when f_{z3} shifts to the other side of passband the first passband and two TZs will be canceled, due to different coupling coefficients for bands 1 and 2.

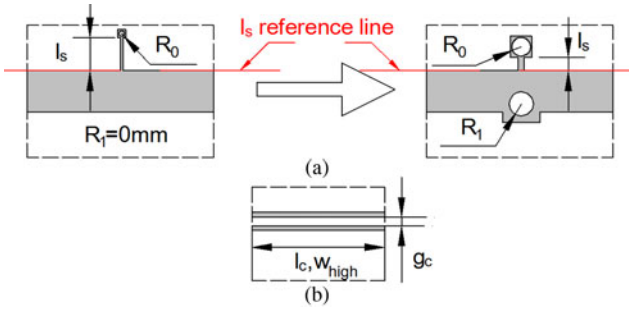

Fig. 5. The structures of: (a) magnetic *K* inverters and (b) capacitive *J* inverter.

III. FILTER DESIGN AND MEASUREMENT

Based on the analysis in Section II, two demonstrative dual-band BPF are designed. In filter A, two pairs of TZs are distributed at two sides of the passbands; in filter B, f_{z2} is redistributed from the upper stopband to the lower stopband of band 1, while f_{z3} is shifted closer to the passband of band 2. The center frequencies and the fractional bandwidths (FBWs) both for filters A and B are $f_{o1} = 0.9$ GHz, $f_{o2} = 1.8$ GHz, $FBW1 = 6.67\%$, and dependent $FBW2 = 8\%$ (based on Q_{e2}), respectively. Thus, $Q_{e1} = 23.5$, dependent $Q_{e2} = 18.9$ (based on Fig. 4), $k_1 = 0.046$, and dependent $k_2 = 0.057$ (based on Fig. 6(a)) can be attained according to a second-order Chebyshev filter with first band return loss $(RL) = 23$ dB [11]. Besides, S–L coupling coefficients, $k_{sl1} = k_{sl2} \approx 0.0002$ for both filters A and B, are optimized as [11]. The synthesized *J*/*K*-invertors, $K_{1A} = 1.48$ ($f_{z2A} \approx 1.3$ GHz), $J_{1A} = 0.0002$ $K_{2A} = 6$ ($f_{z3A} \approx 1.6$ GHz), $J_{2A} = 0.0009$, $K_{1B} = 7.18$ ($f_{z2B} \approx 0.8$ GHz), $J_{1B} = 0.021$, $K_{2B} = 13.68$ ($f_{z3B} \approx 1.75$ GHz), and $J_{2B} = 0.037$, are used according to (2).

The design procedures can be summarized as follow: at first, the initial dimensions of the SIRs are selected based upon [10]: Impedance ratio $R_z = 3$ and electric length ratio $\alpha = 0.5$. Q_{e1} and Q_{e2} can be extracted using the method reported in [11] for the desired center frequencies. Secondly, *K*, *J*, and *k* versus different g_c and l_s (or R_o) can be extracted

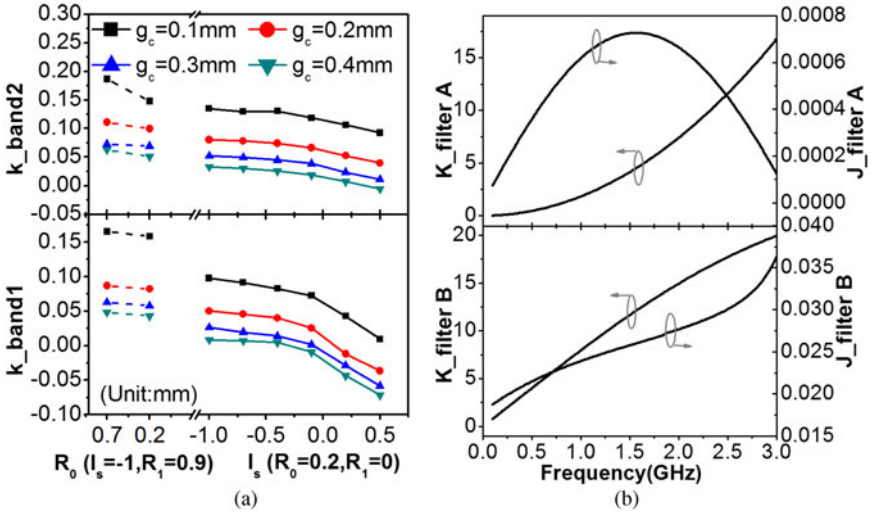

Fig. 6. (a) Impacts of the M-coupling perturbation on the total coupling coefficients *k* of two bands. (b) Extracted *K* and *J* for two cases (all in mm): $R_o = 0.7$, $R_1 = 0.9$, $l_s = -1$, $l_c = 15.8$, $g_c = 0.4$, and $W_{high} = 0.2$ for filter A; and $R_o = 0.2$, $R_1 = 0$, $l_s = -1$, $l_c = 15.9$, $g_c = 0.15$, and $W_{high} = 0.1$ for filter B.

https://doi.org/10.1017/S1759078716001434 Published online by Cambridge University Press

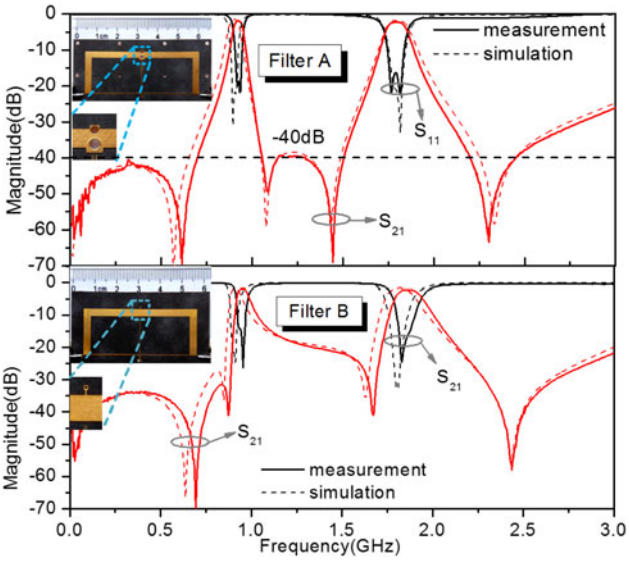

Fig. 8. Simulated and measured *S*-parameters of filters A and B.

using (3) based on the desired first passband, the dependent second passband requirements and central pair of TZs distributions, as depicted in Fig. 5. Then, S–L coupling is added and plotted as Fig. 6 to slightly adjust the central TZs and introduce the other TZ pair. Finally, the filter is optimized by ANSYS HFSS.

The dimensions of filter A are: (all in mm) $W_{to} = 1.54$, $W_t = 0.2$, $W_{high} = 0.2$, $W_{low} = 3.1$, $W_o = 1.6$, $W_1 = 2.8$, $W_2 = 0.8$, $l_{to} = 5$, $l_t = 27.42$, $l_{high} = 43.12$, $l_{low} = 43.02$, $R_o = 0.7$, $R_1 = 0.9$, $R_2 = 0.3$, $l_s = -1$, $l_c = 15.8$, $l_{sl} = 0.9$, $g_{io} = 0.11$, $g_{sl} = 0.2$, and $g_c = 0.4$. The overall size of the filter A is $0.23\lambda_g \times 0.09\lambda_g$, where λ_g denotes the guided wavelength at first-band center frequency. The dimensions of filter B are the same as those of filter A, except for $W_{high} = 0.1$, $l_{high} = 37.925$, $l_{low} = 41.5$, $l_c = 15.9$, $R_o = 0.2$, $R_1 = 0$, $g_c = 0.15$, $l_{sl} = 2$, and $l_s = 0.6$. The overall size of the filter B is $0.21\lambda_g \times 0.09\lambda_g$. Small changes of W_{high}, l_{high}, and l_{low} are made for maintaining the center frequencies and bandwidths.

Figure 8 shows the simulated and the measured results of filters A and B with their photographs. Good agreements between the two filters are observed. Both filters have the same center frequencies and *FBW*, while the distribution of the central TZs (i.e., f_{z2} and f_{z3}) are remarkably different. The center frequencies, insertion losses and FBWs are 0.92/1.8 GHz, 1.8/2.3 dB, and 6.3/7.3% for filter A, and 0.94/1.86 GHz, 1.9/2.1 dB and 7.1/8.6% for filter B, respectively. There are four TZs, $f_{z1A} = 0.6$ GHz, $f_{z2A} = 1.1$ GHz, $f_{z3A} = 1.3$ GHz, and $f_{z4A} = 2.3$ GHz for filter A, and $f_{z1B} = 0.6$ GHz, $f_{z2B} = 0.8$ GHz, $f_{z3B} = 1.6$ GHz, and $f_{z4B} = 2.4$ GHz for filter B. Compared with the synthesized TZ frequencies, $f_{z2A} \approx 1.3$ GHz, $f_{z3A} \approx 1.6$ GHz for filter A, $f_{z2B} \approx 0.8$ GHz and $f_{z3B} \approx 1.75$ GHz for filter B, the measured results are very close to them. The deviation is mainly due to the S–L coupling loading, center frequency shifting, and other parasitic effects.

Table 1 compares the measurement results of some reported high-performance dual-band filter study with those of the proposed work. IL, RL, size, and selectivity of the present study are almost as good as prior works, whereas a pair of optimization-controllable TZ and a pair of synthesis-controllable TZ provide more design freedom for the dual-band passband filter design.

Table 1. Comparison with previous work (TZs and CTZs denote the number of TZ and the number of controllable TZ).

	TZs	CTZs	FBW (%)	IL (dB)	RL (dB)	Size ($\lambda_g \times \lambda_g$)
[3]	4	1 quad	8/5	1.6/2.2	12	0.22 × 0.18
[6]	4	0	8.1/6.8	0.8/1.2	20	0.08 × 0.10
[7]	5	0	14/10	0.8/0.9	20	0.15 × 0.12
[8]	6	0	14/10	1.9/3.4	12	0.09 × 0.09
A	4	2 pairs	6.3/7.3	1.8/2.3	20	0.23 × 0.09
B	4	2 pairs	7.1/8.6	1.9/2.1	15	0.21 × 0.09

IV. CONCLUSION

A novel dual-band BPF with two pairs of controllable TZs has been demonstrated. The synthesis method and adjustment mechanism of the controllable TZ pairs have been mathematically studied and experimentally verified. The filter is constructed by two SIR, MEMC, and S–L coupling, which are utilized to control the center frequencies and two TZ pairs. The admittance graph, derived from coupling coefficient formula, has been employed to mathematically validate the controllability of a TZ pair. The EM simulation has been carried out to verify the controllability of the other TZ pair. Two demonstrative filters with different central TZs distributions and the identical passband performance have been designed. Good agreement between simulation and measurement as well as synthesized TZs consolidate the analysis.

ACKNOWLEDGEMENT

The authors would like to express our sincere thanks to the editors and reviewers of this paper's manuscript for their constructive comments and suggestions, which greatly improved the quality of this paper. The first author Di also thanks Professor Barker in the University of Virginia for his helpful suggestions.

REFERENCES

[1] Mokhtaari, M.; Bornemann, J.; Rambabu, K.; Amari, S.: Coupling-matrix design of dual and triple passband filters. IEEE Microw. Wireless Compon. Lett., **54** (2006), 3490–3492.

[2] Zhang, S.; Zhu, L.: Compact split-type dual-band bandpass filter based on resonators. IEEE Microw. Wireless Compon. Lett., **23** (2013), 344–346.

[3] Zhou, M.; Tang, X.; Xiao, F.: Compact dual band transversal bandpass filter with multiple transmission zeros and controllable bandwidths. IEEE Microw. Wireless Compon. Lett., **19** (2009), 347–349.

[4] Chen, W.; Zhao, Y.-J.; Zhou, X.-J.: Compact and high selectivity dual-band dual-mode microstrip BPF with folded SIR, in Microwave Workshop Series on Millimeter Wave Wireless Technology and Applications (IMWS) IEEE MTT-S International, 2012.

[5] Chen, F.-C.; Qiu, J.-M.; Wong, S.-W.; Chu, Q.-X.: Dual-band coaxial cavity bandpass filter with helical feeding structure and mixed coupling. IEEE Microw. Wireless Compon. Lett., **25** (2015), 31–33.

https://doi.org/10.1017/S1759078716001434 Published online by Cambridge University Press

[6] Wu, G.; Wang, G.; Liang, J.G.; Gao, X.; Zhu, L.: Miniaturised microstrip dual-band bandpass filter using novel symmetric double-spiral resonators for WLAN application. Electron. Lett., **51** (2015), 1177–1178.

[7] Gao, L.; Zhang, X.Y.: High-selectivity dual-band bandpass filter using a quad-mode resonator with source-load coupling. IEEE Microw. Wireless Compon. Lett., **23** (2013), 474–476.

[8] Wei, X.B.; Shi, Y.; Wang, P.; Liao, J.X.; Xu, Z.Q.; Yang, B.C.: Compact dual-band bandpass filter with improved stopband characteristics. Electron. Lett., **48** (2012), 704–706.

[9] Jiang, W.; Shen, W.; Zhou, L.; Gao, A.-M.; Yin, W.-Y.; Mao, J.-F.: Design of compact dual-band quasi-elliptic filter with high selectivity and wide stopband rejection, in Proc. APMC (2012), Kaohsiung, Taiwan, 4–7.

[10] Zhang, S.-B.; Zhu, L.; Weerasekera, R.: Synthesis of inline mixed coupled quasi-elliptic bandpass filters based on resonators. IEEE Trans. Microw. Theory Tech., **63** (2015), 3487–3493.

[11] Makimoto, M.; Yamashita, S.: Microwave Resonators and Filters for Wireless Communication: Theory, Design and Application, Springer, New York, NY, 2001.

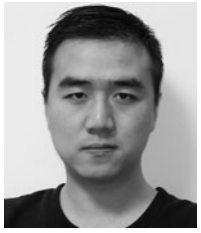

Di Lu was born in Yunnan Province, China, in 1987. He received the B.S. degree in Electronic Engineering School from Chengdu University of Information and Technology (CUIT), China, in 2013. He now is pursuing toward the Ph.D. in University of Science and Technology of China (UESTC). Since October 2015, he has been a Visiting Student with the University of Virginia (UVA). His main research interests are design microwave filters, tunable filters, frequency multipliers, mixers, millimeter-wave circuits, and RF MEMS.

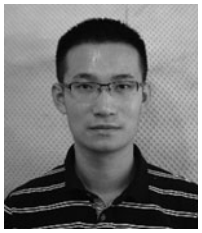

Teng-fei Yan is a Ph.D. student in the Institute of Electronic Engineering, UESTC, from 2012. He is now as a researcher in the Shenzhen Key Laboratory of Millimeter-wave and Wideband Wireless Communications, City University of Hong Kong Shenzhen Research Institute, Shenzhen.

Xiao-hong Tang received B.S. and Ph.D. degrees in Electromagnetism and Microwave technology in UESTC. Now he is a Professor in UESTC. He has authored more than 100 journal and conference papers. He was also the recipient of several national and provincial awards. His research interests include microwave and millimeter communication, computational electromagnetics, etc.

https://doi.org/10.1017/S1759078716001434 Published online by Cambridge University Press